Subsurface bending and reorientation of tilted vortex lattices in bulk isotropic superconductors due to Coulomb-like repulsion at the surface

E. Herrera, I. Guillamón, J. A. Galvis, A. Correa, A. Fente, S. Vieira, H. Suderow, A. Yu. Martynovich, and V. G. Kogan

Subsurface bending and reorientation of tilted vortex lattices in the bulk isotropic superconductors due to Coulomb-like repulsion at the surface

E. Herrera,[1] I. Guillamón,[1] J.A. Galvis,[2, 3] A. Correa,[4] A. Fente,[1]

S. Vieira,[1] H. Suderow,[1] A. Yu. Martynovich,[5] and V. G. Kogan[5]

[1]*Laboratorio de Bajas Temperaturas y Altos Campos Magnéticos,*
Unidad Asociada UAM/CSIC, Departamento de Física de la Materia Condensada,
Instituto de Ciencia de Materiales Nicolás Cabrera, Instituto de Física de la Materia Condensada,
Universidad Autónoma de Madrid, E-28049 Madrid, Spain
[2]*Departamento de ciencias naturales, Facultad de ingenieria y ciencias básicas, Universidad Central, Bogotá, Colombia.*
[3]*National High Magnetic Field Laboratory, Florida State University, Tallahassee, FL 32310, USA.*
[4]*Instituto de Ciencia de Materiales de Madrid, Consejo Superior de Investigaciones Científicas, CSIC, E-28049 Madrid, Spain*
[5]*Ames Laboratory and Department of Physics & Astronomy, Iowa State University, Ames, Iowa 50011, USA*
(Dated: August 28, 2017)

We study vortex lattices (VLs) in superconducting weak-pinning platelet-like crystals of β-Bi$_2$Pd in tilted magnetic fields with a Scanning Tunneling Microscope. We show that vortices exit the sample perpendicular to the surface and are thus bent beneath the surface. The structure and orientation of tilted VL in the bulk are, for large tilt angles, strongly affected by Coulomb-type intervortex repulsion at the surface due to stray magnetic fields.

INTRODUCTION

Rotation in superfluids and superconductors occurs along lines of quantized vortices oriented perpendicular to the rotation plane. Vortex lines tend to be straight to minimize the energy, but they can bend for a variety of reasons, such as supercurrents, fluctuations or interfaces. For instance the vortex liquid phase that appears in cuprate superconductors at high temperatures consists of dynamically fluctuating bent vortices[1]. Bent vortices have been observed in superfluid helium[2] and in Bose Einstein condensates for a range of angular velocities and condensate shapes[3–5]. However, vortex bending has never been directly observed in a superconductor. Scanning tunneling microscopy (STM) is one of the most powerful tools to view vortices, because it shows the vortex lattice at high magnetic fields and in real space. To view bent vortices using STM, one has to create a situation where vortices curve close to the surface. In isotropic superconductors, vortices are expected to exit perpendicular to the surface and should be thus bent when applying tilted magnetic fields[6–8]. Here we study vortices in magnetic fields tilted with respect to the surface of the isotropic superconductor $\beta-$Bi$_2$Pd. We find that the whole vortex lattice bends so that all vortices exit perpendicular to the surface. We also find that the interaction at the sample surface due to stray fields plays a decisive role for the bulk vortex lattice structure.

We study vortex lattices (VLs) at the plane surface of platelet-like single crystals of β-Bi$_2$Pd with $T_c = 5\,$K at low temperatures, $T = 0.15$ K[9, 10]. The crystalline lattice is tetragonal and the Fermi surface has sheets of mixed Bi and Pd orbital character that lead to a near-isotropic macroscopic behavior [11–13]. Upper critical fields along the basal plane and perpendic-

ular to it differ by barely 25% from $H_{c2,ab} = 0.7\,$T to $H_{c2,c} = 0.53\,$T (at low temperatures), leading to coherence lengths $\xi_c = 19\,$nm and $\xi_{ab} = 24\,$nm [14, 15]. Estimates of the penetration depths from the data on the lower critical field give $\lambda_{ab} = 105\,$nm and $\lambda_c = 132\,$nm [14].

EXPERIMENTAL

We use a home-built STM attached to the dilution refrigerator inserted in a three axis vector magnet reaching $5\,$T in the z direction and $1.2\,$T for x and y [16, 17]. β-Bi$_2$Pd crystals ($3 \times 3 \times 0.5\ mm^3$) are mounted with the c-axis along the z direction of the magnet. The other two crystalline orientations with respect to x and y of the magnet are found by scanning the surface with atomic resolution to find the square Bi lattice as outlined in [15]. We provide the in-plane direction of the magnetic field using the azimuthal angle φ, which gives the angle between the in-plane component of the magnetic field and the x axis of the STM scanning window. Crystal growth is described in Ref.[15]. The surface consists of large atomically flat areas of several hundreds nm in size, separated by step edges [15]. We use an Au tip cleaned and atomically sharpened in-situ by repeated indentations onto Au sample [18]. VL images are obtained by mapping the zero-bias conductance normalized to voltages above the superconducting gap [19]. All measurements are done at $T = 150$ mK. Data are usually acquired within field-cooled protocol, although, due to weak pinning of this material, we find the same results when changing the magnetic field at low temperatures. No filtering or image treatment is applied to the conductance maps shown below.
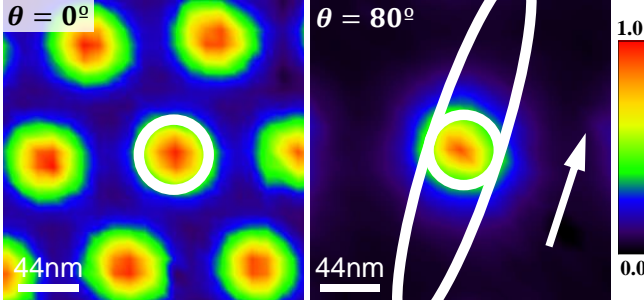
FIG. 1. Zero-bias conductance maps for $H = 0.3\,\mathrm{T}$, $T = 0.15\,\mathrm{K}$; $\theta = 0°$ (left) and $\theta = 80°$ (right). Vortex cores in both cases are roughly circles of the same size. White circles have radii ~ 24 nm. The white ellipse has the major semi-axis of $24/\cos\theta\,\mathrm{nm} = 138$ nm. The arrow indicates the tilt direction. Color bar represents the normalized tunneling conductance for both images.

RESULTS

Vortex bending

Let us consider the vortex core shape at the surface. At $H \parallel c$, the vortex cores of β-$\mathrm{Bi}_2\mathrm{Pd}$ have a circular shape. The core size is of ≈ 24 nm at 0.3 T [20], as shown in Fig. 1 by the white circle. If the vortex in a tilted field would have arrived to the surface being straight without any bending, the expected core shape at the surface would be close to an ellipse with the minor and major semiaxes of 24 nm and $24/\cos\theta$ nm (θ is the angle between $\boldsymbol{H}$ and $\boldsymbol{c}$). For $\theta = 80°$ we would obtain the white ellipse shown in the right panel of Fig. 1. Instead we find the vortex core of the same shape and size as for $\boldsymbol{H}$ normal to the surface as shown by the circle at the right panel of Fig. 1. Thus, our images show that vortices must bend under the surface and exit the sample being perpendicular to the surface.

Vortex bending is expected to occur over a length of the order of the penetration depth $\lambda \approx 100$ nm [6, 7], which is large relative to the core size of 24 nm. Hence, we do not expect that the electronic density of states at the surface is influenced by the bent part of the vortex deep underneath.

The surface VLs are shown in Fig. 2(a) for a few tilts θ. The panel 2(b) shows that, as expected, the density of vortices at the surface goes as $\cos\theta$.

Coulomb-like vortex repulsion at the surface in isotropic superconductors

We construct now a simple model to describe VLs in tilted fields in *isotropic* superconductors. The model predictions, by and large, agree with the STM data. Within this model, the VL in the vortex frame of an infinite sam-
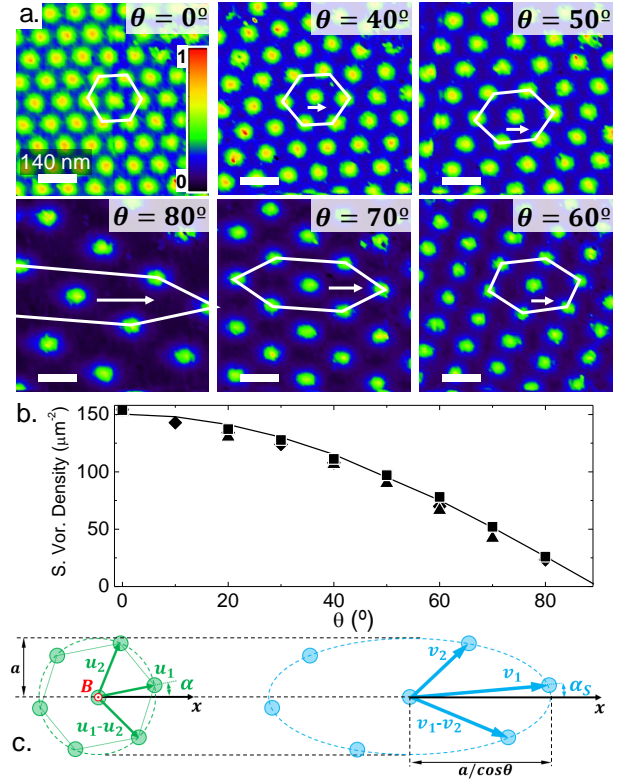

FIG. 2. (a) Zero-bias density of states showing VLs for a few tilt angles θ. The color scale on the top-left panel represents the normalized conductance. White arrows indicate tilt directions. White distorted hexagons are projections onto the surface of hexagonal VLs in the bulk. (b) Density of vortices at the surface vs θ and the normal component of the magnetic induction $H\cos\theta$ (solid curve); different symbols represent different experiments. We use large fields, so that the difference between the applied field $\boldsymbol{H}$ and the magnetic induction $\boldsymbol{B}$ can be disregarded. (c) Schematic representation of the bulk VL in the vortex frame (left panel) with lattice vectors u_1 and u_2 and its surface projection (right panel) with lattice vectors v_1 and v_2 for the tilt along x.

ple is hexagonal and *degenerate*: the angle α shown on the left of Fig. 2(c) can be taken as the degeneracy parameter. The circle where all nearest neighbors are located has a radius a fixed by the flux quantization, $a^2 = 2\phi_0/\sqrt{3}H$. We use the vortex coordinate frame (x, y, z) with z along the vortex direction and the x axis in the tilt plane. For a given α, the VL unit cell vectors (in units of a) are

$$\boldsymbol{u}_1 = [\cos\alpha, \sin\alpha], \quad \boldsymbol{u}_2 = \left[\cos\left(\alpha + \frac{\pi}{3}\right), \sin\left(\alpha + \frac{\pi}{3}\right)\right]. \tag{1}$$

In a sample much thicker than λ, the VL structure in the bulk is dominated by the bulk interactions, i.e. the VL is still hexagonal. However, the degeneracy of the orientation of the bulk vortex lattice with respect to α can be removed by the intervortex interactions at the surface, particularly for high tilt angles.

To see this, we consider that vortices close to the surface interact mainly through the stray magnetic field. We note that due to subsurface bending the point of vortex exit is shifted relative to the exit point extrapolated by straight lines following the bulk vortex lattice. In small fields when the vortices are well separated, each one will experience the same shift. We assume that shifts are the same also in fields of our interest. In particular, this implies that the density of bent vortices at the surface is the same as if vortices were straight; this is consistent with the macroscopic boundary condition for the normal component of the magnetic induction $H \cos \theta$. Hence, the arrangement of vortices at the surface is just shifted relative to the VL which would have been there without subsurface bending. Then, considering the VL structure, one can disregard the bending and the bulk nearest neighbors will be situated at the cross-section of a circular cylinder of radius a with the flat surface, i.e. at the ellipse with semi-axes $a/\cos \theta$ and a, the right panel of Fig. 2c. Taking again the x axis of the surface frame in the tilt plane, one obtains new unit cell vectors at the surface (in units of a):

$$\boldsymbol{v}_1 = \left[\frac{\cos \alpha}{\cos \theta}, \sin \alpha \right], \ \boldsymbol{v}_2 = \left[\frac{\cos(\alpha + \pi/3)}{\cos \theta}, \sin \left(\alpha + \frac{\pi}{3} \right) \right]. \tag{2}$$

In particular, the angle α_s between $\boldsymbol{v}_1$ and $\hat{\boldsymbol{x}}$ is related to the parameter α by $\tan \alpha_s = \tan \alpha \cos \theta$. All vortex positions at the surface $\boldsymbol{R}_{mn} = m\boldsymbol{v}_1 + n\boldsymbol{v}_2$ (m, n are integers) can be expressed in terms of θ and α (or α_s).

We can now treat the stray fields out of the sample as created by point "monopoles" producing the magnetic flux ϕ_0 in the free space within the solid angle 2π. The interaction energy of the vortex at the origin with the rest is

$$\frac{\phi_0^2}{4\pi^2} \sum_{m,n} {}' \frac{1}{R_{mn}}, \tag{3}$$

where $\sum'$ is over all m, n except $m = n = 0$. The surface vortex density is $H \cos \theta / \phi_0$, so that surface interaction per cm^2 is

$$F_s = \frac{\phi_0 H \cos \theta}{4\pi^2} \sum_{m,n} {}' \frac{1}{R_{mn}} = \frac{3^{1/4} \phi_0^{1/2} H^{3/2}}{4\sqrt{2}\pi^2} S(\alpha, \theta), \tag{4}$$

$$S = \cos^2 \theta \sum_{m,n} {}' \left\{ [m \cos \alpha + n \cos(\alpha + \pi/3)]^2 \right.$$

$$\left. + \cos^2 \theta [m \sin \alpha + n \sin(\alpha + \pi/3)]^2 \right\}^{-1/2}. \tag{5}$$

It is readily checked that $\partial S / \partial \alpha = 0$ at $\alpha = -\pi/6$ and $\pi/3$. The corresponding structures in the vortex frame are hexagons, called hereafter A and A'; in A two out of six nearest neighbors are at y axis, in A' they are at x.

The sum S is divergent and as such depends on the summation domain. We, however, are interested only in

the angular dependence of $S(\alpha)$, because of its role in removing the VL degeneracy in the bulk. The angular dependence arises mostly due to vortices in the vicinity of the central one, because the number of far-away vortices grows with the distance and their combined contribution to the interaction is nearly isotropic. Our strategy for evaluation of $S(\alpha)$ is based on the fact that the Coulomb interaction out of the sample is isotropic and therefore we can do the summation within a circle $R_{mn} < L$, where L is large enough to include a few "nearest-neighbor shells" of vortices surrounding the one at the origin. To provide a smooth truncation we add a factor $e^{-R_{mn}^2/L^2}$ to the summand of Eq. (5).

Results of these calculations are given in Fig. 3 for $\theta \approx 80°, 70°$ and $60°$; smaller tilt angles are discussed in the Appendix. Clearly, the structure A ($\alpha = -\pi/6$) is
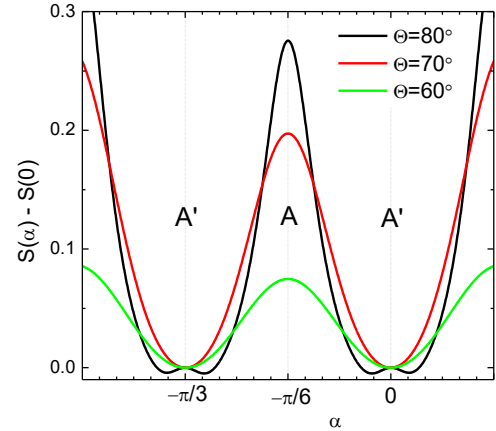

FIG. 3. The surface energy angular dependence $S(\alpha) - S(0)$ for $\theta = 80°(black), 70°(red), 60°(green)$ for $L = 4$ and $-15 < m, n < 15$. Curves $S(\alpha)$ are shifted vertically to have the same zero value at $\alpha = 0$. The curve $\theta = 80°$ is in fact asymmetric relative to $\alpha = 0$ with the absolute minimum at $\alpha \approx -0.1$.

unstable. The minimum energy for $\theta = 70°$ and $60°$ is at $\alpha = 0$, so that the preferred structure is A'. For $\theta = 80°$ the minimum is shifted to $\alpha \approx -0.1$. These qualitative conclusions do not change if one takes a larger radius L of the summation domain, notwithstanding the increase of the calculated surface energy F_s.

Comparison with experiment and reorientation of the vortex lattice

To show that our model describes the data well, and in particular to check again that the bulk hexagonal VL projects onto the surface as if the vortices were straight, one can follow the bulk nearest neighbors and their surface projections. The six nearest neighbors in the vortex

frame correspond to the pairs (m, n):

$$(0, 1), \ (1, 0), \ (0, -1), \ (-1, 0), \ (-1, 1), \ (1, -1). \quad (6)$$

At the surface, these pairs mark six vortex positions situated at $\pm\boldsymbol{v}_1$, $\pm\boldsymbol{v}_2$, and $\pm(\boldsymbol{v}_1 - \boldsymbol{v}_2)$, see the sketch in Fig. 2c. These positions at the surface are not necessarily nearest, because at large tilt angles, they form a strongly stretched hexagon, whereas the position $(1, 1)$, moves closer to the center.

Let us consider $\theta = 80°$ for which according to Fig. 3 $\alpha \approx -0.1$ and evaluate distances $d_1 = |\boldsymbol{v}_1|$, $d_2 = |\boldsymbol{v}_2|$, and $d_3 = |\boldsymbol{v}_1 - \boldsymbol{v}_2|$. Skipping algebra, we provide formulas for these distances in the Appendix. In units of a we obtain $(d_1, d_2, d_3) = (5.68, 3.56, 2.63)$. Direct measurements at the corresponding image at Fig. 2a give $(d_1, d_2, d_3) \approx (6, 3.4, 2.4)$ in a good agreement with calculated values. Hence, the VL in the bulk bends as a whole when reaching the surface, just shifting the geometric projection of the tilted hexagonal bulk VL onto the surface, and loses its degeneracy by arranging with the angle α that minimizes the interaction due to stray fields.

In Fig. 4 we show α for experiments changing the in-plane direction of the magnetic field (for a tilt of $\theta = 80°$). We observe that the orientation fluctuates around A'. The deviations from A' can be caused by vortex pinning or by the tetragonal symmetry of the crystalline lattice, not included in our model.

DISCUSSION

As shown in previous work, VLs in $\beta-\mathrm{Bi}_2\mathrm{Pd}$ in fields along c are hexagonal up to H_{c2} with one of the VL vectors along a or b of the tetragonal crystal [15]. This gives a two-fold degeneracy in the VL orientation [21], with domains of differently oriented VLs. In some tetragonal materials in fields along c, the four-fold-symmetric nonlocal corrections to the London theory modify the isotropic repulsion and lead to two degenerate rhombic VLs which at large fields transform to the square VL [22, 23]. One of the requirements for the nonlocal corrections to work is a large Ginzburg-Landau parameter κ [24]. In our crystals, $\kappa \sim 4$ and we do not observe VL transitions. Interestingly, at highly tilted fields, the surface intervortex interaction is strong enough to remove the degeneracy observed in fields along c between the two vortex lattice orientations and fix the degeneracy parameter α such that the surface interaction energy is minimized.

We recall that materials with extreme anisotropies such as $\mathrm{Bi}_2\mathrm{Sr}_2\mathrm{CaCu}_2\mathrm{O}_\delta$ reveal Josephson vortex lattices crossing with lattices of 2D pancake vortices. Lorentz microscopy on vortices pinned to columnar defects that were tilted with respect to the surface (the magnetic field being applied perpendicular to the surface) have been studied in $\mathrm{Bi}_2\mathrm{Sr}_2\mathrm{CaCu}_2\mathrm{O}_\delta$[25]. Elongated images with
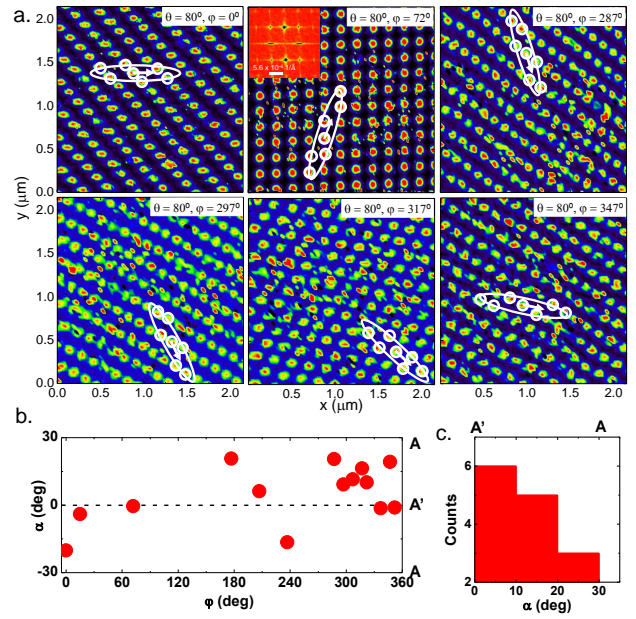

FIG. 4. In a we show VLs for a fixed tilt $\theta = 80°$ but different directions of the in-plane component of the magnetic field, characterized by azimuthal angles φ. VLs are made of vortices strongly bent under the surface. Note that these lattices are still very well ordered, in spite of the vortex bending. Color scale is the same as in Figs. 1,2. In b we show the angle α (defined in Fig. 2c) obtained for images made at a polar angle of $\theta = 80°$ as a function of φ. In c we accumulate the absolute values of α in three ranges, from low α, close to the A' orientation to higher α close to the A orientation.

a contrast decreased with respect to perpendicular vortices are found when pinning of pancake vortices to the tilted columnar defects is strong. Further measurements in tilted magnetic fields in the same system show crossing Josephson and pancake vortex lattices, chain vortices, kinked structures of pancakes, as well as flux cutting in non-equilibrium situations [26–33]. On the other hand, measurements in high purity Nb crystals in tilted magnetic fields show that the bulk VL has a variety of structural transitions, including two-fold structures breaking the crystalline four-fold rotation symmetry and scalene unit cells[34]. The Ginzburg-Landau $\kappa \sim 1$ and the observed structures probably show anisotropic features of the Fermi surface of Nb[34]. Tilted VLs have been also studied in 2H-NbSe$_2$, showing distorted hexagons whose orientation disagrees with theoretical expectations [35–40]. It was proposed that vortex-induced strain of the crystal might explain the data [41]. At high tilt angles, buckling transitions produce superlattices with chain-like vortex arrangements [37, 38]. Besides, vortex cores have star-like shapes in fields along c and acquire comet-like tails in tilted fields, making it difficult to find the vortex core size in this material. The anisotropy in all these ma-

terials ranges from the highly anisotropic pancake vortex situation of the cuprates, to the isotropic vortices of Nb, passing through the intermediate situation of 2H-NbSe$_2$. No true vortex bending has been seen in these systems, either because the bending scale is as short as the inter-layer spacing in highly anisotropic systems with pancake vortices, or because other effects, such as the influence of the anisotropy of the Fermi surface, have been considered. Our work show that the way vortex cores behave close to the surface can be relevant in every situation in tilted fields, and contributes to the vortex interactions in the bulk.

In summary, we have studied VLs in tilted fields in the isotropic superconductor β-Bi$_2$Pd. We demonstrate that vortices exit the sample being perpendicular to the surface, that necessitates the subsurface bending of vortex lines. We find that intervortex Coulomb-like repulsion at the surface due to stray fields removes the degeneracy of the bulk hexagonal VLs thus fixing the bulk VL orientation.

ACKNOWLEDGEMENTS

APPENDIX

Vortex lattices at the surface

Within the *isotropic* model, the VL in the vortex frame of an infinite sample is hexagonal and *degenerate*: the angle α shown on the left panel of Fig. 2(c) can be taken as the degeneracy parameter. For a given α, the VL
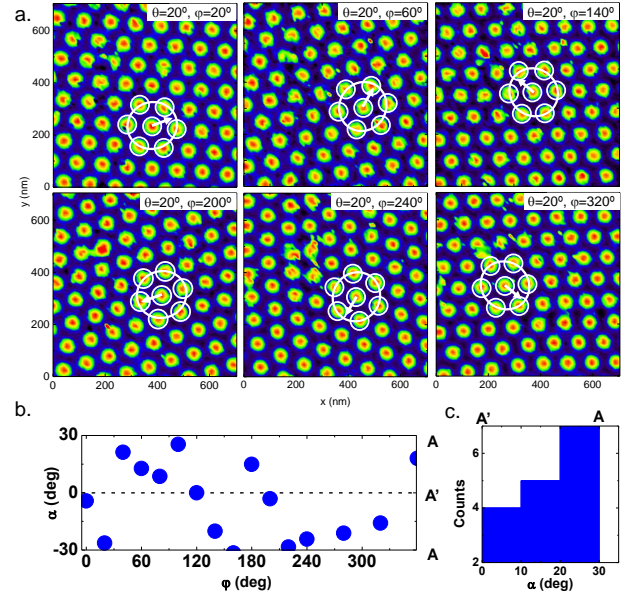

FIG. 5. In a we show zero bias conductance maps for a polar angle of $\theta = 20°$ and different in-plane directions of the magnetic field, characterized by azimuthal angles φ. We mark a few vortex hexagons by six white circles. These are joined by white ellipses, following Fig. 2c. As the polar tilt is so small, the ellipticity is hardly seen in the figure. White arrows represent the projection of the magnetic field in the plaine, or φ (counted counterclockwise starting from the positive x-axis, as shown in Fig. 2c). In b we show the angle α vs φ. When counting values of α and distributing their absolute value in three angular ranges, we find the histogram shown in c.

unit cell vectors (in units of a) are given by the Eq. (1). Positions of the nearest neighbors are $\pm\boldsymbol{u}_1$, $\pm\boldsymbol{u}_2$, and $\pm(\boldsymbol{u}_1 - \boldsymbol{u}_2)$, all of them at the same distance $d = 1$ from the vortex at the origin.

It is argued in the main text that considering the VL structure, one can disregard the vortex bending. Then, the bulk nearest neighbors will be situated at the cross-section of a circular cylinder of radius a with the surface plane, i.e. at the ellipse with semi-axes $a/\cos\theta$ and a (right panel of Fig. 2c). Taking the x axis of the surface frame in the tilt plane, one obtains new unit cell vectors at the surface (in units of a) given by Eq. (2).

The positions corresponding to the bulk nearest neighbors are $\pm\boldsymbol{v}_1$, $\pm\boldsymbol{v}_2$, and $\pm(\boldsymbol{v}_1-\boldsymbol{v}_2)$. These positions at the surface are not necessarily the nearest. Their distances from the vortex at the origin are $d_1 = |\boldsymbol{v}_1|$, $d_2 = |\boldsymbol{v}_2|$, and $d_3 = |\boldsymbol{v}_1 - \boldsymbol{v}_2|$. For these distances one has:

$$d_1^2 = \frac{\cos^2\alpha + \cos^2\theta\sin^2\alpha}{\cos^2\theta} \, , \tag{7}$$

$$d_2^2 = \frac{\cos^2(\alpha + \pi/3) + \cos^2\theta\sin^2(\alpha + \pi/3)}{\cos^2\theta} \, , \tag{8}$$

$$d_3^2 = \frac{[\cos(\alpha + \pi/3) - \cos\alpha]^2}{\cos^2\theta} + \left[\sin\left(\alpha + \frac{\pi}{3}\right) - \sin\alpha\right]^2 . \tag{9}$$

We provide in 42 a code calculating the vortex arrangements that can be expected on the surface, according to these equations.

It is worth mentioning that the VL at the surface is always a strongly distorted hexagon. Accordingly, there can be angles θ at which the surface VL is nearly a square. For instance, we can see that the A' configuration with $\alpha = 0.1$ leads to a square surface VL for $\theta = 78°$. This can be obtained by considering the vectors $\boldsymbol{s}_1 = \boldsymbol{v}_1 - \boldsymbol{v}_2$ and $\boldsymbol{s}_2 = \boldsymbol{v}_2 + (\boldsymbol{v}_2 - \boldsymbol{v}_1)$. For $\theta \approx 78°$ these are perpendicular, $\boldsymbol{s}_1 \cdot \boldsymbol{s}_2 = 0$. A careful examination of this condition leads to the conclusion that the square lattice can be obtained for $\theta \geq 74°$. For $\theta = 74°$, the square lattice is obtained at $\alpha = -\pi/12$. With increasing θ, there are two values of α, symetrically positioned around $\alpha = -\pi/12$ where the square lattice is obtained. The separation between these values of α increases and, for $\theta \to 90°$ $\alpha \to 0$ and $-\pi/6$. It is noteworthy that we only observe square-like lattices when α is small, further supporting that the vortex lattice tends to orient along A', as shown by our model calculations.

Low polar angles

From Fig. 3 one can see that the structure A ($\alpha = -\pi/6$) is unstable since the energy has a maximum at this configuration. Moreover, this feature does not depend on the number of neighbors included in the summation. Hence, we expect that for relatively small tilts, minimum energy shown in Fig. 3 corresponds to small α (along with α_S) i.e., the VL structure is close to A'. For $\theta = 0.5 \approx 28.6°$, the distances d_i are 1.14, 1.04, 1.04, all three are larger than 1, as expected because of the Coulomb repulsion. Note that for the lattice A, there will be one of the d_i equal to 1. Thus, even the smallest intervortex distance at the surface exceeds the bulk intervortex distance a.

We examine now experiments for a polar angle $\theta = 20°$. The result of the experiment is shown in Fig.5a. Here, the vortex lattice remains practically undistorted. In Fig.5b we show α for $\theta = 20°$ and different in-plane directions of the magnetic field. As we see in Fig.5, the angle α strongly fluctuates between A and A', with some tendency to orient along A. This suggests that, for this angle, the surface Coulomb interaction is competing with the bulk two-fold degeneracy between A and A'. Possibly other effects as the interaction with the crystalline lattice and pinning, which we do not take into account in our model, also play a relevant role.

Vortex core shape as a function of the bias voltage

When increasing the bias voltage up from zero bias to the superconducting gap, the vortex core shape slightly changes, as discussed in previous work for perpendicular magnetic fields[15, 20]. The shape observed in the STM slightly spreads out when reaching the gap edge. This is shown in the top row in Fig. 6. In β-Bi$_2$Pd, the gap edge is located at about 0.7 mV. The vortex is practically undetectable in conductance maps at bias voltages close to the gap edge, because, for this bias voltage just below the gap and when the tunneling conductance is close to its value at high bias voltages, the conductance inside and outside the vortex core is practically the same. For bias voltages below but close to this value, the vortex core shape occupies a larger portion of the image. This is shown in the Fig. 6 and has been explained by the superfluid currents around the vortex core. These Doppler shift the gap edge towards slightly lower bias voltages [43–45]. Then, at a distance from the core where the currents are large, the density of states increases for bias voltages just below the gap edge (at, say 0.6 mV), effectively leading to an increased vortex core radius. When the field is nearly parallel, the bias voltage dependence of the vortex core is the same as for perpendicular fields (bottom of Fig. 6). This suggests that the current distribution around the vortex core is not altered by the parallel magnetic field, confirming again vortex bending.

———————————

[1] G. Blatter, M. V. Feigel'man, V. B. Geshkenbein, A. I. Larkin, and V. M. Vinokur. Vortices in high-temperature superconductors. *Rev. Mod. Phys.*, 66:1125–1388, Oct 1994. doi:10.1103/RevModPhys.66.1125. URL http://link.aps.org/doi/10.1103/RevModPhys.66.1125.

[2] Gregory P. Bewley, Matthew S. Paoletti, Katepalli R. Sreenivasan, and Daniel P. Lathrop. Characterization of reconnecting vortices in superfluid helium. *Proceedings of the National Academy of Sciences*, 105(37):13707–13710, 2008. doi:10.1073/pnas.0806002105. URL http://www.pnas.org/content/105/37/13707.abstract.

[3] P. Rosenbusch, V. Bretin, and J. Dalibard. Dynamics of a single vortex line in a Bose-Einstein condensate. *Phys. Rev. Lett.*, 89:200403, Oct 2002. doi:10.1103/PhysRevLett.89.200403. URL https://link.aps.org/doi/10.1103/PhysRevLett.89.200403.

[4] Alexander L. Fetter. Rotating trapped Bose-Einstein condensates. *Rev. Mod. Phys.*, 81:647–691, May 2009. doi:10.1103/RevModPhys.81.647. URL https://link.aps.org/doi/10.1103/RevModPhys.81.647.

[5] J. J. García-Ripoll and V. M. Pérez-García. Vortex bending and tightly packed vortex lattices in Bose-Einstein condensates. *Phys. Rev. A*, 64:053611, Oct 2001. doi:10.1103/PhysRevA.64.053611. URL https://link.aps.org/doi/10.1103/PhysRevA.64.053611.

[6] E.H. Brandt. Tilted and curved vortices in anisotropic superconducting films. *Phys. Rev. B*, 48:6699, 1993.

[7] A. Martynovich. Magnetic vortices in layered superconducting slabs. *Zh. Eksp. Teor. Fis.*, 105:912, 1994.

[8] Ivan A. Sadovskyy, Ying Jia, Maxime Leroux, Jihwan Kwon, Hefei Hu, Lei Fang, Carlos Chaparro, Shaofei Zhu, Ulrich Welp, Jian-Min Zuo, Yifei Zhang, Ryusuke

Nakasaki, Venkat Selvamanickam, George W. Crabtree, Alexei E. Koshelev, Andreas Glatz, and Wai-Kwong Kwok. Toward superconducting critical current by design. *Advanced Materials*, 28(23):4593–4600, 2016. ISSN 1521-4095. doi:10.1002/adma.201600602. URL http://dx.doi.org/10.1002/adma.201600602.

[9] Yoshinori Imai, Fuyuki Nabeshima, Taiki Yoshinaka, Kosuke Miyatani, Ryusuke Kondo, Seiki Komiya, Ichiro Tsukada, and Atsutaka Maeda. Superconductivity at 5.4 K in β-Bi$_2$Pd. *Journal of the Physical Society of Japan*, 81(11):113708, 2012. doi:10.1143/JPSJ.81.113708. URL http://dx.doi.org/10.1143/JPSJ.81.113708.

[10] N. Alekseevski, N. Zhuravlev, and I. Lifanov. *Zh. Eksp. Teor. Fiz.*, 125:27, 1954.

[11] I. R. Shein and A. L. Ivanovskii. Electronic band structure and fermi surface of tetragonal low-temperature superconductor β-Bi$_2$Pd as predicted from first principles. *Journal of Superconductivity and Novel Magnetism*, 26(1):1–4, 2013. ISSN 1557-1947. doi:10.1007/s10948-012-1776-x. URL http://dx.doi.org/10.1007/s10948-012-1776-x.

[12] M. Sakano and et al. Topologically protected surface states in a centrosymmetric superconductor β-Bi$_2$Pd. *Nat Comm*, 6(8595), October 2015. doi:10.1038/ncomms9595. URL http://www.nature.com/ncomms/2015/151013/ncomms9595/pdf/ncomms9595.pdf.

[13] A. Coldea. Unpublished. 2016.

[14] J. Kačmarčík, Z. Pribulová, T. Samuely, P. Szabó, V. Cambel, J. Šoltýs, E. Herrera, H. Suderow, A. Correa-Orellana, D. Prabhakaran, and P. Samuely. Single-gap superconductivity in β-Bi$_2$Pd. *Phys. Rev. B*, 93:144502, Apr 2016. doi:10.1103/PhysRevB.93.144502. URL http://link.aps.org/doi/10.1103/PhysRevB.93.144502.

[15] E. Herrera, I. Guillamón, J. A. Galvis, A. Correa, A. Fente, R. F. Luccas, F. J. Mompean, M. García-Hernández, S. Vieira, J. P. Brison, and H. Suderow. Magnetic field dependence of the density of states in the multiband superconductor β-Bi$_2$Pd. *Phys. Rev. B*, 92:054507, Aug 2015. doi:10.1103/PhysRevB.92.054507. URL http://link.aps.org/doi/10.1103/PhysRevB.92.054507.

[16] H. Suderow, I. Guillamón, and S. Vieira. Compact very low temperature scanning tunneling microscope with mechanically driven horizontal linear positioning stage. *Review of Scientific Instruments*, 82(3):033711, 2011. URL http://scitation.aip.org/content/aip/journal/rsi/82/3/10.1063/1.3567008.

[17] J.A. Galvis, E. Herrera, I. Guillamón, J. Azpeitia, R.F. Luccas, C. Munuera, M. Cuenca, J.A. Higuera, N. Díaz, M. Pazos, M. García-Hernández, A. Buendía, S. Vieira, and H. Suderow. Three axis vector magnet set-up for cryogenic scanning probe microscopy. *Rev. Sci. Inst.*, 86: 013706, 2015. doi:http://dx.doi.org/10.1063/1.4905531. URL http://scitation.aip.org/content/aip/journal/rsi/86/1/10.1063/1.4905531.

[18] J. G. Rodrigo, H. Suderow, and S. Vieira. *European Phys. Journal B*, 40:483, 2004.

[19] I. Guillamón, H. Suderow, S. Vieira, L. Cario, P. Diener, and P. Rodière. Superconducting density of states and vortex cores of 2H-NbS$_2$. *Phys. Rev. Lett.*, 101:166407, Oct 2008. doi:10.1103/PhysRevLett.101.166407. URL http://link.aps.org/doi/10.1103/PhysRevLett.101.166407.

[20] A. Fente, E. Herrera, I. Guillamón, H. Suderow, S. Mañas Valero, M. Galbiati, E. Coronado, and V. G. Kogan. Field dependence of the vortex core size probed by scanning tunneling microscopy. *Phys. Rev. B*, 94:014517, Jul 2016. doi:10.1103/PhysRevB.94.014517. URL http://link.aps.org/doi/10.1103/PhysRevB.94.014517.

[21] Barbara Gränz, Sergey E. Korshunov, Vadim B. Geshkenbein, and Gianni Blatter. Competing structures in two dimensions: Square-to-hexagonal transition. *Phys. Rev. B*, 94:054110, Aug 2016. doi:10.1103/PhysRevB.94.054110. URL http://link.aps.org/doi/10.1103/PhysRevB.94.054110.

[22] M. R. Eskildsen, K. Harada, P. L. Gammel, A. B. Abrahamsen, N. H. Andersen, G. Ernst, A. P. Ramirez, D. J. Bishop, K. Mortensen, D. G. Naugle, K. D. D. Rathnayaka, and P.C. Canfield. *Nature*, 393:242–245, 1998.

[23] M. Yethiraj, D. K. Christen, D. McK. Paul, P. Miranovic, and J. R. Thompson. Flux lattice symmetry in V_3Si: Nonlocal effects in a high-κ superconductor. *Phys. Rev. Lett.*, 82:5112–5115, Jun 1999. doi:10.1103/PhysRevLett.82.5112. URL http://link.aps.org/doi/10.1103/PhysRevLett.82.5112.

[24] V. G. Kogan, M. Bullock, B. Harmon, P. Miranovic, Lj. Dobrosavljevic Grujic, P. L. Gammel, and D. J. Bishop. Vortex lattice transitions in borocarbides. *Phys. Rev. B*, 55:R8693–R8696, Apr 1997.

[25] A. Tonomura, H. Kasai, O. Kamimura, T. Matsuda, K. Harada, Y. Nakayama, J. Shimoyama, K. Kishio, T. Hanaguri, K. Kitazawa, M. Sasase, and S. Okayasu. Observation of individual vortices trapped along columnar defects in high-temperature superconductors. *Nature*, 412(6847):620–622, Aug 2001. ISSN 0028-0836. doi:10.1038/35088021. URL http://dx.doi.org/10.1038/35088021.

[26] A. Tonomura, H. Kasai, O. Kamimura, T. Matsuda, K. Harada, T. Yoshida, T. Akashi, J. Shimoyama, K. Kishio, T. Hanaguri, K. Kitazawa, T. Masui, S. Tajima, N. Koshizuka, P. L. Gammel, D. Bishop, M. Sasase, and S. Okayasu. Observation of structures of chain vortices inside anisotropic high-T_c superconductors. *Phys. Rev. Lett.*, 88:237001, May 2002. doi:10.1103/PhysRevLett.88.237001. URL https://link.aps.org/doi/10.1103/PhysRevLett.88.237001.

[27] L. N. Bulaevskii, M. Ledvij, and V. G. Kogan. Vortices in layered superconductors with Josephson coupling. *Phys. Rev. B*, 46:366–380, Jul 1992. doi:10.1103/PhysRevB.46.366. URL https://link.aps.org/doi/10.1103/PhysRevB.46.366.

[28] S. Bending. Local magnetic pprobe of superconductors. *Advances in Physics*, 48(4):449–535, 1999.

[29] A. Tonomura, H. Kasai, O. Kamimura, T. Matsuda, K. Harada, J. Shimoyama, K. Kishio, and K. Kitazawa. Motion of vortices in superconductors. *Nature*, 397(6717):308–309, Jan 1999. ISSN 0028-0836. doi:10.1038/16826. URL http://dx.doi.org/10.1038/16826.

[30] A. Tonomura, H. Kasai, O. Kamimura, et al. Observation of Structures of Chain Vortices Inside Anisotropic High-Tc Superconductors. *Phys. Rev. Lett.*, 88(237001): 2002. doi:10.1103/PhysRevLett.88.237001. URL https://doi.org/10.1103/PhysRevLett.88.237001.

[31] M. Beleggia, G. Pozzi, A. Tonomura, et al. Model of superconducting vortices in layered materials for the interpretation of transmission electron microscopy

images. *Phys. Rev. B*, 70(184518):2004. doi: 10.1103/PhysRevB.70.184518. URL https://doi.org/10.1103/PhysRevB.70.184518.

[32] A. Buzdin and I. Baladié. Attraction between pancake vortices in the crossing lattices of layered superconductors. *Phys. Rev. Lett.*, 88:147002, Mar 2002. doi: 10.1103/PhysRevLett.88.147002. URL http://link.aps.org/doi/10.1103/PhysRevLett.88.147002.

[33] A. E. Koshelev. Tilted and crossing vortex chains in layered superconductors. *Journal of Low Temperature Physics*, 139(1):111–125, 2005. ISSN 1573-7357. doi:10.1007/BF02769571. URL http://dx.doi.org/10.1007/BF02769571.

[34] S. Mühlbauer, C. Pfleiderer, P. Böni, M. Laver, E. M. Forgan, D. Fort, U. Keiderling, and G. Behr. Morphology of the superconducting vortex lattice in ultrapure niobium. *Phys. Rev. Lett.*, 102:136408, Apr 2009. doi: 10.1103/PhysRevLett.102.136408. URL http://link.aps.org/doi/10.1103/PhysRevLett.102.136408.

[35] C. A. Bolle, F. De La Cruz, P. L. Gammel, J. V. Waszczak, and D. J. Bishop. Observation of tilt induced orientational order in the magnetic flux lattice in 2H-NbSe$_2$. *Phys. Rev. Lett.*, 71:4039–4042, Dec 1993. doi: 10.1103/PhysRevLett.71.4039. URL http://link.aps.org/doi/10.1103/PhysRevLett.71.4039.

[36] P. L. Gammel, D. A. Huse, R. N. Kleiman, B. Batlogg, C. S. Oglesby, E. Bucher, D. J. Bishop, T. E. Mason, and K. Mortensen. Small angle neutron scattering study of the magnetic flux-line lattice in single crystal 2H-NbSe$_2$. *Phys. Rev. Lett.*, 72:278–281, Jan 1994. doi: 10.1103/PhysRevLett.72.278. URL http://link.aps.org/doi/10.1103/PhysRevLett.72.278.

[37] H.F. Hess, C.A. Murray, and J.V. Waszczak. Scanning tunneling microscopy study of distortion and instability of inclined flux line lattice structures in the anisotropic superconductor 2H-NbSe$_2$. *Phys. Rev. Lett.*, 69:2138, 1992.

[38] H. F. Hess, C.A. Murray, and J. V. Waszczak. Flux lattice and vortex structure in 2H-NbSe$_2$ in inclined fields. *Phys. Rev. B*, 50:16528, 1994.

[39] I. Fridman, C. Kloc, C. Petrovic, and J.Y.T. Wei. Lateral imaging of the superconducting vortex lattice using doppler-modulated scanning tunneling microscopy. *Appl Phys Lett*, 99:192505, 2011.

[40] I. Fridman, C. Kloc, C. Petrovic, and J.Y.T. Wei. *ArXiV*, page 1303.3559, 2013.

[41] V. G. Kogan, L. N. Bulaevskii, P. Miranović, and L. Dobrosavljević-Grujić. Vortex-induced strain and flux lattices in anisotropic superconductors. *Phys. Rev. B*, 51:15344–15350, Jun 1995. doi: 10.1103/PhysRevB.51.15344. URL http://link.aps.org/doi/10.1103/PhysRevB.51.15344.

[42] URL https://github.com/LowTemperaturesUAM/Tilted-Vortex-Lattice.

[43] A. Kohen, Th. Proslier, T. Cren, Y. Noat, W. Sacks, H. Berger, and D. Roditchev. Probing the superfluid velocity with a superconducting tip: The doppler shift effect. *Phys. Rev. Lett.*, 97:027001, Jul 2006. doi: 10.1103/PhysRevLett.97.027001. URL https://link.aps.org/doi/10.1103/PhysRevLett.97.027001.

[44] A. Maldonado, S. Vieira, and H. Suderow. Supercurrent on a vortex core in 2H-NbSe$_2$: Current-driven scanning tunneling spectroscopy measurements. *Phys. Rev. B*, 88:064518, Aug 2013. doi:10.1103/PhysRevB.88.064518. URL https://link.aps.org/doi/10.1103/PhysRevB.88.064518.

[45] C. Berthod. Quasiparticle spectra of Abrikosov vortices in a uniform supercurrent flow. *Phys. Rev. B*, 88:134515, Oct 2013. doi:10.1103/PhysRevB.88.134515. URL https://link.aps.org/doi/10.1103/PhysRevB.88.134515.
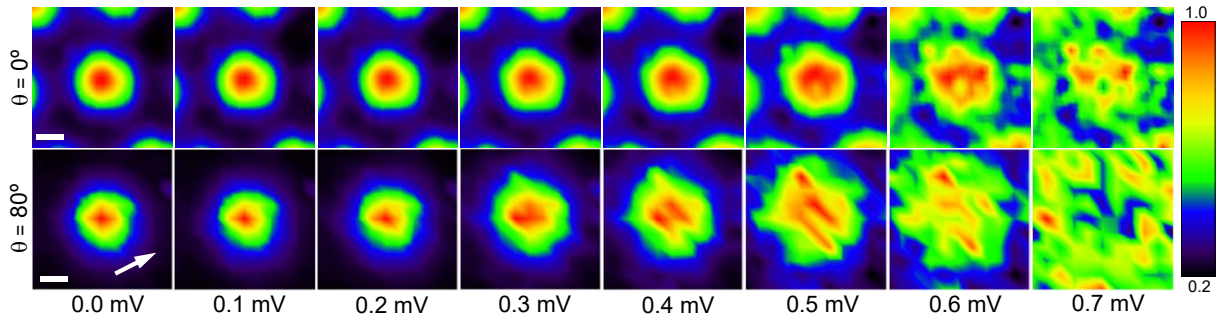
FIG. 6. Conductance map of single vortices for perpendicular fields ($\theta = 0°$, upper row) and strongly tilted magnetic fields ($\theta = 80°$, bottom row). Color scale is given by the bar on the right. The bias voltage for each conductance map is provided in the bottom of the figure. The arrow in the bottom left panel provides the in-plane direction of the magnetic field. White horizontal bars are of 25 nm.